第32卷第12期 焊 接 学 报 Vol. 32 No. 12
2011年12月 TRANSACTIONS OF THE CHINA WELDING INSTITUTION December 2011

Sn-Cu-Ni 焊点纳米压痕试验分析

王俭辛， 赖忠民， 孙丹丹
（江苏科技大学 先进焊接技术省级重点实验室，镇江 212003）

摘 要： 为研究金属间化合物与无铅焊点力学性能之间的关系，采用纳米压痕法测定了 Sn-Cu-Ni 焊点中金属间化合物及钎料基体的弹性模量和压痕硬度等力学性能参量. 结果表明，Sn-Cu-Ni 焊点中 $(Cu,Ni)_6Sn_5$ 金属间化合物的弹性模量为 113.2 GPa ± 4.8 GPa，压痕硬度为 5.59 GPa ± 0.32 GPa，均与钎料基体有较大差异. 并基于 Mayo-Nix 方法计算得到 Sn-Cu-Ni，Sn-Cu-Ni-0.05Ce 和 Sn-Pb 钎料基体的蠕变应变速率敏感指数 m 分别为 0.128 6，0.124 8 和 0.183 2，蠕变应力指数 n 分别为 7.776 0，8.012 8 和 5.458 5，表明 Sn-Cu-Ni 系列抗蠕变性能优于 Sn-Pb 钎料，且微量 Ce 元素的添加有利于提高 Sn-Cu-Ni 焊点的抗蠕变性能.

关键词： 无铅钎料； 纳米压痕； 弹性模量； 蠕变应变速率敏感指数
中图分类号： TG454 **文献标识码：** A **文章编号：** 0253－360X(2011)12－0059－04

王俭辛

0 序 言

20 世纪末纳米压痕仪的出现，为薄膜材料的力学性能测定提供了新方法、新途径. 压痕法原本是一种用来测试材料硬度的传统试验方法，由于压痕试验设备得到了重大改进，可以连续记录压头压入材料过程中的载荷与压入深度的变化，即获得压入载荷与压入深度之间的连续曲线——$F-h$ 曲线，由此提出并发展了纳米压痕(nanoindentation)技术，通过分析从中获得材料的弹性模量等力学性能参量[1]. Mayo 等人[2,3]利用纳米压痕技术测定了 TiO_2 与 ZnO 等材料的纳米压痕硬度、弹性模量，并通过理论计算，得到其蠕变性能参量.

近年来，纳米压痕试验方法被引入到微电子焊接领域，研究集中在 Sn-Ag-Cu 体系上[4-8]，得到了 Sn-Ag-Cu 焊点的压痕硬度、弹性模量等力学性能参量. 试验针对波峰焊工艺中 Sn-Pb 钎料的主要替代品——Sn-Cu-Ni 体系展开研究，测试分析焊点中金属间化合物以及钎料基体的压痕硬度、弹性模量等参量，并基于 Mayo-Nix 方法研究蠕变速率敏感指数及蠕变应力敏感指数等蠕变性能参量，以期为该体系钎料的进一步推广应用提供借鉴.

收稿日期：2010－07－15
基金项目：江苏高校优势学科建设工程资助项目；江苏省高校“青蓝工程”科技创新团队资助项目；江苏省先进焊接技术重点实验室开放研究基金资助项目(10622011501)

1 试验方法

试验选用纯锡，纯铜以及 Sn-Ni，Sn-Ce 中间合金制备 Sn-0.5Cu-0.05Ni (-0.05Ce) 钎料合金，将 Sn-Cu-Ni(-Ce) 及 Sn-Pb 钎料预成形，置于待钎焊部位，再使用 HT-990 型红外再流焊机将 0805(2.03 mm × 1.27 mm) 型矩形片式电阻元件钎焊在印刷电路板上.

钎焊后利用 SHIMADZU(岛津) 的 DUH-W201S 型纳米压痕仪对焊点进行压痕试验，压痕仪的压头为 115°的三棱锥压头. 为保证压痕试验中试样表面平整，将待测试样进行磨平、抛光并清洗干净. 在加载过程中，压头以 2 mN/s 的速率压入材料表面，当载荷达到预先设定的最大值 F_m(50 mN) 后保持一段时间然后卸载，对焊点中的金属化合物 $(Cu,Ni)_6Sn$ 和 Sn-0.5Cu-0.05Ni(-0.05Ce) 钎料基体分别进行多次纳米压痕试验，最大载荷保持时间分别为 5 s 和 3 min.

2 力学性能参数确定

加载和卸载的压痕过程中载荷－位移($F-h$)曲线示意图见图 1，F_{max} 和 h_{max} 分别为最大载荷和最大压入深度，h_f 为卸载后的残余深度，上段卸载曲线的切线斜率 S 为弹性接触刚度，切线与坐标轴的交点位移定义为 h_c.

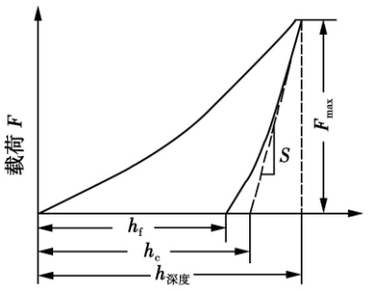

图 1 加载及卸载过程中载荷—位移曲线

Fig. 1 Typical force-displacement ($F-h$) curve during loading and unloading

从 $F-h$ 曲线中可得到 h_c 与 S 等重要参量，由此，弹性模量与压痕硬度可由以下关系来确定[4,5]，即

$$H=\frac{F_{\max}}{A} \tag{1}$$

$$E_r=\frac{\sqrt{\pi}}{2\beta}\cdot S\cdot\frac{1}{\sqrt{A}} \tag{2}$$

$$\frac{1}{E_r}=\frac{1-v^2}{E}+\frac{1-v_i^2}{E_i} \tag{3}$$

式中：H 为试样的压痕硬度；A 为压痕的投影面积；E_r 为约化的弹性模量；β 为已知的压头修正系数；E 和 v 分别为试样的弹性模量和泊松比；E_i 和 v_i 分别为已知的压头弹性模量和泊松比. 压痕仪的压头为 115°的三棱锥，由几何关系得到

$$A=26.43h_c^2 \tag{4}$$

从而可确定试样的弹性模量 E 与压痕硬度 H. 由于钎料的服役温度已超过其熔化温度的一半，且焊点的可靠性与钎料蠕变性能有很大关系，因而即使在室温也不得不考虑蠕变的影响. 以往分析蠕变性能的方法多是采用单轴拉伸蠕变试验，这需要制备较多试样，而采用纳米压痕技术则使得在小体积钎料上研究其蠕变性能成为可能.

从载荷—位移曲线进行分析，在最大载荷 F_m 处保持一段时间，如压入深度继续增加则说明材料发生了蠕变，载荷保持期间的压入深度即蠕变位移. 通过对 $F-h$ 曲线进行研究可得到钎料的蠕变性能参量，假设蠕变特征可由以下方程表示，即

$$\dot{\varepsilon}=\frac{\sigma}{E}+b\sigma^n \tag{5}$$

或

$$\sigma=E\varepsilon+b'\dot{\varepsilon}^m \tag{6}$$

式中：$\dot{\varepsilon}$ 为蠕变应变速率；m 为蠕变速率敏感指数；n 为蠕变应力敏感指数；b，b' 为材料结构相关的系数.

根据 Mayo-Nix 方法[2,3]，蠕变时间较长时，可得到蠕变时间—蠕变位移的关系曲线（图 2），图 2 中曲线可分为两部分，初始蠕变阶段和大位移阶段. 在初始阶段中，开始时蠕变位移变化很快，随着时间的延长，蠕变位移的变化逐渐变慢，进入大位移阶段后，蠕变位移与蠕变时间呈近似线性关系，这为物理分析推导蠕变速率敏感指数提供了可能，故研究中对钎料基体的载荷保持时间设置为 3 min，以满足该分析方法的需要.

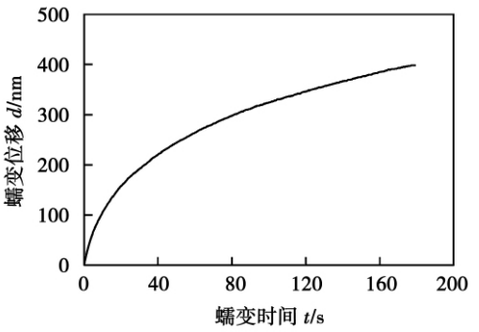

图 2 压痕过程中蠕变时间—蠕变位移示意图

Fig. 2 Relation of creep deformation versus dwell time

对蠕变时间—蠕变位移曲线，在其后期的近似线性阶段采集数据计算得到[2-4]

$$\dot{\varepsilon}=\frac{1}{d}\cdot\frac{\mathrm{d}d}{\mathrm{d}t} \tag{7}$$

式中：d 为保持阶段的压入深度，即蠕变位移；t 为蠕变时间. 从而得到近似线性阶段 H 与 $\dot{\varepsilon}$ 的关系数据，将蠕变结果表示成两者的双对数曲线，经数据拟和确定出的直线斜率即蠕变应变速率敏感指数[2-4]

$$m=\frac{\mathrm{d}\ln\sigma}{\mathrm{d}\ln\dot{\varepsilon}}=\frac{\mathrm{d}\ln H}{\mathrm{d}\ln\dot{\varepsilon}} \tag{8}$$

$$n=\frac{1}{m} \tag{9}$$

根据 Mayo-Nix 方法研究蠕变速率敏感指数及蠕变应力敏感指数等蠕变性能，具有测试方法简便，而且推导结果并不受加载速度影响等优点.

3 试验结果与分析

对 Sn-Cu-Ni 焊点中的金属间化合物 $(Cu,Ni)_6Sn_5$ 进行了多次纳米压痕试验，图 3 列出了压痕过程中典型的载荷—位移曲线，从而可得到其压痕硬度为 5.59 GPa ± 0.32 GPa，弹性模量为 113.2 GPa ± 4.8 GPa，这与 Sn-Ag-Cu 焊点中 Cu_6Sn_5 化合物的力学性能参量相差无几[6,7].

图 4 分别为 Sn-Cu-Ni，Sn-Cu-Ni-0.05Ce 和 Sn-Pb 钎料基体在压痕过程中的载荷—位移曲线. 从多次测试中得到Sn-Cu-Ni，Sn-Cu-Ni-0.05Ce和Sn-Pb

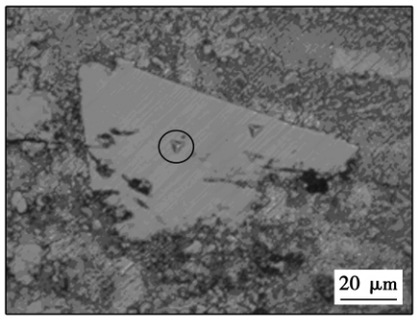

(a) 压痕形貌

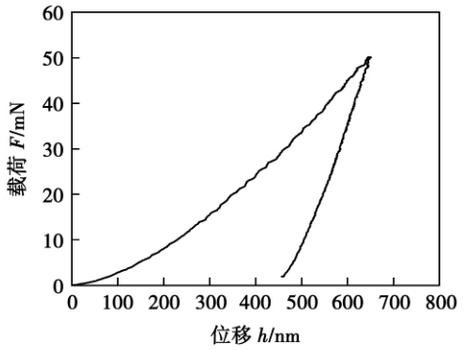

(b) 载荷–位移曲线

图 3　$(Cu,Ni)_6Sn_5$ 纳米压痕试验结果

Fig. 3　Nanoin dentation measurement for $(Cu,Ni)_6Sn_5$

钎料基体的压痕硬度分别是 159.2 MPa ± 20.4 MPa，165.8 MPa ± 18.2 MPa 和 154.8 MPa ± 21.4 MPa，弹性模量分别为 46.4 GPa ± 4.6 GPa，48.2 GPa ± 3.8 GPa 和 24.6 GPa ± 2.4 GPa.

通过分析 Sn-Cu-Ni 焊点中金属间化合物以及钎料基体的压痕硬度和弹性模量可知，$(Cu,Ni)_6Sn_5$ 的压痕硬度比基体大一个数量级，弹性模量是基体的两倍多，说明使金属间化合物发生一定弹性变形的应力比钎料基体要大的多，即在一定应力作用下，金属间化合物发生的弹性变形较小.

在最大载荷保持阶段，各曲线中均出现一平台，说明在载荷恒定时压入深度随时间延长而继续增加，即钎料发生了蠕变，平台部分即蠕变位移. 在最大载荷保持阶段所产生的蠕变时间—蠕变位移曲线见图 5，从图 5 中可知，在最大载荷保持阶段，Sn-Cu-Ni 系列钎料基体的蠕变位移要小于 Sn-Pb 钎料，而微量 Ce 元素的添加可减少 Sn-Cu-Ni 的蠕变.

根据 Mayo-Nix 方法，可得到如图 6 所示的压痕硬度与蠕变应变速率的对数关系，经数据拟和确定出直线斜率即蠕变应变速率敏感指数 m，Sn-Cu-Ni，Sn-Cu-Ni-0.05Ce 和 Sn-Pb 钎料基体的 m 值分别为 0.128 6，0.124 8 和 0.183 2，折算成蠕变应力指数 n 分别为 7.776 0，8.012 8 和 5.458 5，这与传统拉伸蠕变测试所得到的试验结果较相近[8].

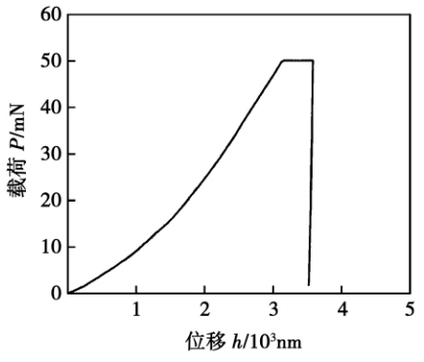

(a) Sn-Cu-Ni

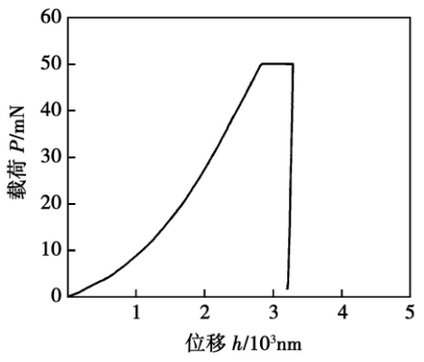

(b) Sn-Cu-Ni-0.05Ce

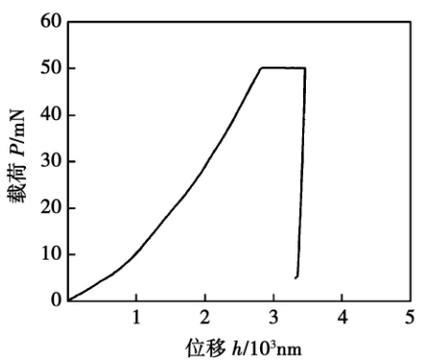

(c) Sn-Pb

图 4　钎料基体载荷—位移曲线

Fig. 4　Force versus displacement for solder alloy

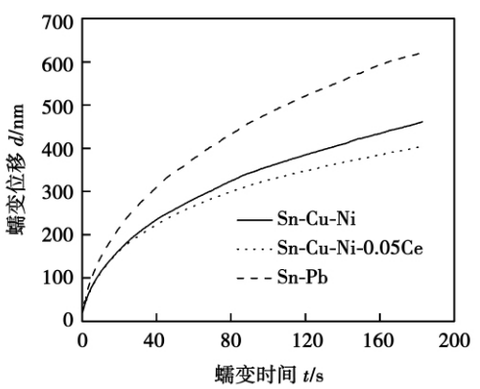

图 5　钎料基体蠕变时间—蠕变位移曲线

Fig. 5　Creep time-depth curves of solder alloy

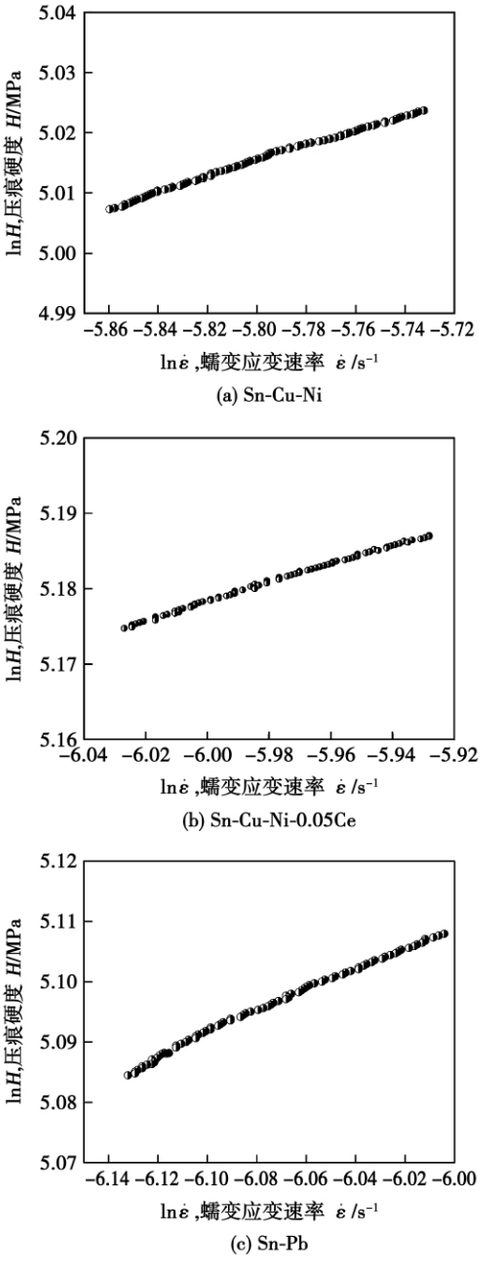

图 6 钎料基体蠕变应变速率—压痕硬度关系图

Fig. 6 Relation of creep strain rate and hardness of solder alloy

Sn-Pb 钎料是由富锡相 + 富铅相构成的固溶体，而 Sn-Cu-Ni 钎料的显微组织是由富锡相 + 金属间化合物构成，细小的金属间化合物颗粒硬度较高，弥散分布于钎料中，能够阻碍位错的滑移，使得抗蠕变性能有较大的提高. 但粗大的金属间化合物由于力学性能参量与钎料基体有较大的差异，因此对整个焊点的力学性能将起到负面作用.

微量 Ce 元素可聚集在表面、界面处，有效降低界面能，阻碍晶界滑动，因此对焊点抗蠕变性能具有显著改善作用，试验结果表明添加 Ce 元素可有效提高 Sn-Cu-Ni 焊点的抗蠕变性能.

4 结 论

(1) Sn-Cu-Ni 焊点中 $(Cu,Ni)_6Sn_5$ 金属间化合物的弹性模量为 113.2 GPa ± 4.8 GPa，压痕硬度为 5.59 GPa ± 0.32 GPa，与钎料基体相差较大.

(2) 通过理论计算，得到 Sn-Cu-Ni，Sn-Cu-Ni-0.05Ce 和 Sn-Pb 钎料基体的蠕变应变速率敏感指数 m 分别为 0.128 6，0.124 8 和 0.183 2，蠕变应力指数 n 分别为 7.776 0，8.012 8 和 5.458 5.

(3) 从抗蠕变性能来看，Sn-Cu-Ni 系列抗蠕变性能优于 Sn-Pb 钎料，在 Sn-Cu-Ni 钎料中添加微量 Ce 元素，可获得抗蠕变性能更优的焊点.

参考文献:

[1] Joslin D L, Oliver W C. A new method for analyzing data from continuous depth-sensing microindentation tests [J]. Journal of Materials Research, 1990, 5(1): 123 – 126.

[2] Mayo M J, Siegel R W, Narayanasamy A, *et al*. Mechanical properties of nanophase TiO_2 as determined by nanoindentation [J]. Journal of Materials Research, 1990, 5(5): 1073 – 1082.

[3] Mayo M J, Siegel R W, Liao Y X, *et al*. Nanoindentation of nanocrystalline ZnO [J]. Journal of Materials Research, 1992, 7(4): 973 – 979.

[4] Gao F, Nishikawa H, Takemoto T, *et al*. Mechanical properties versus temperature relation of individual phases in Sn-3.0Ag-0.5Cu lead-free solder alloy [J]. Microelectronics Reliability, 2009, 49(3): 296 – 302.

[5] Chromik R R, Vinci R P, Allen S L, *et al*. Measuring the mechanical properties of Pb-free solder and Sn-based intermetallics by nanoindentation [J]. Journal of the Minerals, Metals and Materials Society, 2003, 55(6): 66 – 69.

[6] Dudek M A, Chawla N. Nanoindentation of rare earth-Sn intermetallics in Pb-free solders [J]. Intermetallics, 2010, 18(5): 1016 – 1020.

[7] Chandra Rao B S S, Weng J, Shen L, *et al*. Morphology and mechanical properties of intermetallic compounds in SnAgCu solder joints [J]. Microelectronic Engineering, 2010, 87(11): 2416 – 2422.

[8] 王凤江，钱乙余，马 鑫. 纳米压痕法测量 Sn-Ag-Cu 无铅钎料 BGA 焊点的力学性能参数 [J]. 金属学报，2005，41(7)：775 – 779.
Wang Fengjiang, Qian Yiyu, Ma Xin. Measurement of mechanical properties of Sn-Ag-Cu bulk solder BGA solder joint using nanoindentation [J]. Acta Metallrugica Sinica, 2005, 41(7): 775 – 779.

作者简介： 王俭辛，男，1981 年出生，博士，讲师. 主要研究方向为无铅钎料及微电子焊接技术. 发表论文 10 篇. Email: wangjx_just@126.com

Through comparing the simulation results and experimental measurements, the prediction accuracy of the developed thermo-elastic-plastic FEM based on Quick Welder was verified. Meanwhile, the influence of welding sequence on the residual stress distribution was clarified using numerical simulation method. The results show that both transverse residual stress and longitudinal residual stress were significantly affected by deposition sequence. The deposition sequence not only largely changes the peak values of residual stress, but also alters the shape of residual stress distribution.

Key words: numerical simulation; non-linear analysis; welding residual stress; welding sequence

Nanoindentation measurement of Sn-Cu-Ni joint WANG Jianxin, LAI Zhongmin, SUN Dandan (Province Key Lab of Advanced Welding Technology, Jiangsu University of Science and Technology, Zhenjiang 212003, China). p 59 - 62

Abstract: In order to study the effect of intermetallic compound on mechanical properties of joint, the elastic modulus and hardness of intermetallic compounds were analyzed by nanoindentation method, and the creep strain rate sensitivity of solder matrix was obtained by Mayo-Nix method. From the physical analysis of nanoindentation curves, the elastic modulu of $(Cu, Ni)_6Sn_5$ in Sn-Cu-Ni joints is 113.2 GPa ± 4.8 GPa, while the hardness is 5.59 GPa ± 0.32 GPa. It is found that intermetallic compounds are the key factors in the reliability of lead-free joints, due to the big contrasts between mechanical properties of intermetallic compounds and solder matrix. The creep strain rate sensitivities of Sn-Cu-Ni, Sn-Cu-Ni-0.05Ce and Sn-Pb solder matrix are 0.1286, 0.1248, and 0.1832, and the creep stress exponents are 7.7760, 8.0128, and 5.4585, respectively, which indicate the improvement in creep resistance of Sn-Cu-Ni joints due to Ce addition.

Key words: lead-free solder; nanoindentation; elastic modulu; creep strain rate sensitivity

Interfacial microstructure of sintering composites of PCBN grains-graphite particles-CuSnTi alloy ZHANG Bin, DING Wenfeng, XU Jiuhua, CHEN Zhenzhen, SU Honghua, FU Yucan (College of Mechanical and Electrical Engineering, Nanjing University of Aeronautics and Astronautics, Nanjing 210016, China). p 63 - 65, 69

Abstract: Sintering experiments of Cu-Sn-Ti alloy, polycrystalline cubic boron nitride (PCBN) abrasive grains and graphite particles were carried out at the heating temperature of 920 ℃ with the dwell time of 30 min. The strength of sintering bulks was measured by means of the three-point bending experiments. The interfacial microstructure and the phases of the sintering bulks were characterized using scanning electron microscope (SEM), energy dispersion spectrometer (EDS) and X-ray diffraction (XRD). The results reveal that in the case of the graphite content of 5 ~ 15 wt%, the bending strength of the composite bulks is above 91 MPa, which is much higher than that of the bulk strength of the vitrified grinding wheels. The elemental diffusion behavior has taken place across the joining interface between PCBN grains and Cu-Sn-Ti alloy in the sintering process. The compounds were formed, therefore, the PCBN grains were bonded firmly. Under such condition, the breakage of the PCBN grains has played the most important role in the fracture of the composite bulks. In particular, the breakage mode of the PCBN grains is the intergranular fracture.

Key words: PCBN abrasive grains; Cu-Sn-Ti alloy; bending strength; interfacial microstructure

Finite element analysis of temperature field during keyhole-plasma arc welding using SYSWELD software HU Qingxian[1], WANG Yanhui[1], YAO Qingjun[2], WANG Shunyao[1] (1. Provincial Key Lab of Advanced Welding Technology, Jiangsu University of Science and Technology, Zhenjiang 212003, China; 2. Jiangsu Province Special Equipment Safety Supervision Inspection Institute, Yangzhou Branch, Yangzhou 225003, China). p 66 - 69

Abstract: Considering the weld geometric characters of keyhole plasma arc welding (K-PAW), a suitable and adaptive combined heat source for numerical simulation is developed, i.e. at the transverse cross-section and along the workpiece thickness direction, the double-ellipsoidal volumetric heat source acts at upper part of the workpiece while a linearly-increased peak value of heat flux in gaussian cylinder mode exerts at lower part of the workpiece. Based on the developed adaptive combined heat source model, the welding temperature field of 6 mm thickness stainless steel is simulated by SYSWELD. The predicted weld geometry and fusion line locus at cross-section are in good agreement with the experimental measurement. This demonstrates the suitability of the combined volumetric heat source mode.

Key words: keyhole plasma arc welding; temperature field; combined volumetric heat source; finite element analysis

Study on ultrasonic stir hybrid welding of aluminum alloy HE Diqiu, LI Jian, LI Donghui, LIANG Jianzhang (State Key Laboratory of High-performance Complex Manufacturing, Central South University, Changsha 410083, China). p 70 - 72, 108

Abstract: Friction stir welding (FSW) of aluminum alloy usually results in a special "funnel shaped" temperature field, which makes obvious difference of microstructure properties in the direction of weld seams. In order to get better properties of welded joints, ultrasonic stir hybrid welding technology has been put forward in this paper, which concentrates the ultrasonic energy in deep weld seams through the stirring pin. Thickness of 2.5 mm 2219 aluminum alloy sheets has been adopted and welded by the two technologies mentioned above in this experiment, microstructure and mechanical properties of weld are analyzed and compared as well. Result shows that the weld joints of 2219 aluminum welded by the two technologies are both with good appearance and defect-free in the inner, and ultrasonic stir hybrid welding obviously has better mechanical properties.

Key words: ultrasonic stir hybrid welding; friction stir welding; 2219 aluminum alloy

Effect of Nd addition on microstructure and mechanical property of Sn3.8Ag0.7Cu solder joint GAO Lili, XUE Songbai, WANG Bo (College of Materials Science and Technology, Nanjing University of Aeronautics and Astronautics, Nanjing 210016, China). p 73 - 76

Abstract: The effects of Nd addition(0, 0.05, 0.5wt%) on the microstructure and shear strength of SAC solder joint under as-reflowed and 150 ℃ isothermal-aging process were investigated. Experimental results showed that Nd addition can obviously improve the shear strength and microstructure of the SAC solder joints. The growth rate of the SAC/Cu interfacial layer as